PNAS RESEARCH ARTICLE | BIOPHYSICS AND COMPUTATIONAL BIOLOGY

Cholesterol inhibits human voltage-gated proton channel hHv1

Shuo Han[a], Xiang-Ping Chu[b], Ryan Goodson[a], Prae Gamel[a], Sophia Peng[a], Joshua Vance[a], and Shizhen Wang[a,1]

Edited by Ehud Isacoff, University of California, Berkeley, CA; received March 28, 2022; accepted July 20, 2022

Although human sperm is morphologically mature in the epididymis, it cannot fertilize eggs before capacitation. Cholesterol efflux from the sperm plasma membrane is a key molecular event essential for cytoplasmic alkalinization and hyperactivation, but the underlying mechanism remains unclear. The human voltage-gated proton (hHv1) channel functions as an acid extruder to regulate intracellular pHs of many cell types, including sperm. Aside from voltage and pH, Hv channels are also regulated by distinct ligands, such as Zn^{2+} and albumin. In the present work, we identified cholesterol as an inhibitory ligand of the hHv1 channel and further investigated the underlying mechanism using the single-molecule fluorescence resonance energy transfer (smFRET) approach. Our results indicated that cholesterol inhibits the hHv1 channel by stabilizing the voltage-sensing S4 segment at resting conformations, a similar mechanism also utilized by Zn^{2+}. Our results suggested that the S4 segment is the central gating machinery in the hHv1 channel, on which voltage and distinct ligands are converged to regulate channel function. Identification of membrane cholesterol as an inhibitory ligand provides a mechanism by which the hHv1 channel regulates fertilization by linking the cholesterol efflux with cytoplasmic alkalinization, a change that triggers calcium influx through the CatSper channel. These events finally lead to hyperactivation, a remarkable change in the mobility pattern indicating fertilization competence of human sperm.

ion channel | structural dynamics | voltage gating | ligand gating | cholesterol

Significance

Our work identified membrane cholesterol as a new inhibitor of human voltage-gated proton channel hHv1. Using single-molecule fluorescence resonance energy transfer (smFRET), we further showed that cholesterol inhibits the hHv1 channel by stabilizing the voltage-sensing S4 segment at resting conformations, a similar mechanism also utilized by Zn^{2+} inhibition. Our findings provided a new mechanism that the hHv1 channel regulates human fertilization by linking the cholesterol efflux with intracellular alkalization, thus sperm hyperactivation.

The sperm in the human epididymis is morphologically matured, but it does not gain the ability to fertilize eggs until residing in female reproductive tracts, where it is capacitated to be fertilization competent (1, 2). During capacitation, sperm membrane cholesterol is depleted by albumin and high-density lipoprotein (HDL) rich in oviductal fluids, through a mechanism that remains to be elucidated (3). The fertilization-competent sperm, however, can be "decapacitated" by incubating with lipid vesicles containing cholesterol (4, 5). Cholesterol efflux was mainly suggested as a mechanism to destabilize the plasma membrane to facilitate sperm–egg fusion (6). But cytoplasmic alkalinization essential for human sperm hyperactivation also depends on cholesterol efflux (1, 2, 7), with the underlying mechanisms remaining unclear. Among the ion channels expressed in sperm, the human voltage-gated proton (hHv1) is a standalone voltage sensor without a separate pore-forming domain (8, 9). The voltage dependence of the hHv1 channel is shifted by the transmembrane pH gradient, therefore normally opening to mediate proton efflux (10). The hHv1 channel is important for the pH homeostasis of many cells, including sperm (10–12). So far, only a few ligands are reported to regulate hHv1 channels, including Zn^{2+}, polyunsaturated arachidonic acid, and albumin (13–15). Ligand regulation of the sperm hHv1 channel plays an important role in the fertilization process. For example, high Zn^{2+} in male seminal fluid inhibits proton efflux through sperm hHv1 channels to suppress NOX5 NADPH oxidase, thus maintaining sperm quiescence (16), while the low Zn^{2+} environment of the female reproductive tract permits the sperm hHv1 channel to open to elevate intracellular pH (17). In fact, intracellular alkalization mediating by the hHv1 channel is a key factor activating the CatSper calcium channel that leads to sperm hyperactivation (17–19). Most recently, albumin rich in female oviductal fluids, except its ability to facilitate cholesterol efflux (1), was reported to directly activate the sperm hHv1 channel (14).

In the present work, we identified cholesterol as an inhibitory ligand of the hHv1 channel. Direct inhibition of the hHv1 channel by cholesterol provides a mechanism that links cholesterol efflux with intracellular alkalization essential for sperm capacitation. To understand how cholesterol inhibits the hHv1 channel, we examined the cholesterol-induced conformational changes of the hHv1 channel using single-molecule fluorescence resonance energy transfer (smFRET). Our data showed that cholesterol stabilizes the S4 segment at resting conformations to suppress channel openings, a mechanism also utilized by Zn^{2+} that was well characterized by multiple approaches (15, 20–23). Our results suggested that the hHv1 channel plays a critical role in sperm

Author affiliations: [a]Division of Biological and Biomedical Systems, School of Science and Engineering, University of Missouri-Kansas City, Kansas City, MO 64110; and [b]Department of Biomedical Sciences, School of Medicine, University of Missouri-Kansas City, Kansas City, MO 64108

Author contributions: S.W. conceived the study; S.W., S.H., and X.-P.C. designed research; S.H., S.P., J.V., R.G., P.G., and X.-P.C. performed research; S.H., X.-P.C., and S.W. analyzed data; and S.W. wrote the paper.

The authors declare no competing interest.

This article is a PNAS Direct Submission.

[1]To whom correspondence may be addressed. Email: wangshizhen@umkc.edu.

This article contains supporting information online at http://www.pnas.org/lookup/suppl/doi:10.1073/pnas.2205420119/-/DCSupplemental.

Published August 29, 2022.

capacitation, with its S4 segment as the central gating machinery that is regulated by voltage, pH, and multiple ligands, including cholesterol and Zn^{2+}.

Results

hHv1 Channel Is Inhibited by Cholesterol. Membrane lipids are essential for the function of many ion channels (24, 25). By working on the hHv1 channels expressed in *Escherichia coli* host cells, we obtained the pure hHv1 proteins that are cholesterol free. We reconstituted the hHv1 protein into liposomes containing lipids 1-palmitoyl-2-oleoyl-sn-glycero-3-phosphoethanolamine (POPE)/1-palmitoyl-2-oleoyl-sn-glycero-3-phospho-(1'-rac-glycerol) (POPG) (3/1, wt/wt) and determined its function using liposome flux assays (26). Driven by the K^+ Nernst potential, the proton uptake into liposomes through hHv1 channels is reported by protonation-induced quenching of 9-amino-6-chloro-2-methoxyacridine (ACMA) fluorescence (Fig. 1*A* and *SI Appendix*, Fig. S1*A*). But the empty liposomes without the hHv1 proteins always exhibited steady ACMA fluorescence until the addition of proton ionophore carbonyl cyanide m-chlorophenyl hydrazine (CCCP) (*SI Appendix*, Fig. S1*A*). In liposomes containing cholesterol, the hHv1 channel was inhibited in a dose-dependent manner, with a half inhibition concentration (IC_{50}) of ~10% (wt/wt, to total membrane lipids) as predicted by the Hill equation, which is well within the membrane cholesterol contents of human sperm and many other cells (Fig. 1 *B* and *C*). Using the enhanced green fluorescent protein (EGFP)-tagged hHv1 channel, we validated that cholesterol inhibition was not the result of altered channel incorporation or orientation into liposomes (*SI Appendix*, Fig. S1 *B* and *C*). Although we cannot rule out cholesterol effects on the oligomeric state of hHv1 channels, extracting cholesterol from liposomes by 5 mM methyl-β-cyclodextrin (β-MCD) indeed remarkably attenuated channel inhibition (Fig. 1 *D* and *E*). Human albumin is also able to extract cholesterol from cell membranes (1, 27). At a concentration of 7.5 μM, which is not sufficient to offer direct activation (14), human albumin was also found to significantly alleviate cholesterol inhibition of hHv1 channels (*SI Appendix*, Fig. S1 *D* and *E*). On HEK293 cells expressing hHv1-EGFP channels, robust proton currents were recorded under whole-cell patch-clamp recording mode (Fig. 1*G*). Exposing the cells to 5 mM β-MCD led to over ~30% of increases in proton currents, which were profoundly inhibited by 0.1 mM extracellular Zn^{2+} (Fig. 1*G*). Statistical analysis of current densities (pA/pF) confirmed that extraction of membrane cholesterol by 5 mM β-MCD promotes hHv1 channel function (Fig. 1*H*). Removal of the N- and carboxyl-terminal cytosolic domains (M1-A75 and R223-N273) does not attenuate cholesterol inhibition of the hHv1 channel (Fig. 1*F*), suggesting that cholesterol acts on the voltage-sensing domain. The function of the purified hHv1 channels was further confirmed using Zn^{2+} (15, 28), by showing that only Zn^{2+}, not Mg^{2+} or Ca^{2+}, inhibit proton uptake through hHv1 channels (Fig. 1*I*). Our data indicated that inhibition of the hHv1 channel by Zn^{2+} was dose dependent (Fig. 1*J*), and the IC_{50} predicted by the Hill equation was 86 μM, very close to those reported by electrophysiological studies (15). Moreover, our data indicated that Zn^{2+} inhibition is highly cooperative with a Hill coefficient of 2, consistent with the previous reports (20). We also tested the effects of many cholesterol analogs on hHv1 channel function (*SI Appendix*, Fig. S2*A*) using concentrations close to their cellular levels (10 μM). Our data indicated that, except for ergosterol from fungi, all the cholesterol analogs tested, including progesterone, estradiol, pregnenolone, desmosterol, and hydroxycholesterol, do not change the hHv1 channel function that could be physiologically significant (*SI Appendix*, Fig. S2*B*).

Cholesterol Inhibits the hHv1 Channel by Stabilizing Close State Conformations. In our previous work, we measured the real time FRET changes between the donor and acceptor fluorophores conjugated at the K125C-S224C and K169C-Q194C labeling sites in the hHv1 channel using smFRET (Fig. 2*A*) (29). We showed that FRET transitions observed from the two different labeling sites reflect the movements of the S4 segment in the hHv1 channel that are associated with voltage and pH gating (29). To uncover the structural basis underlying cholesterol inhibition, we examined the structural changes of the hHv1 channel in liposomes that were induced by 20% cholesterol under different voltages using smFRET.

The smFRET traces collected from the two labeling sites indicated that the S4 segment transit among three conformational states, which were the low (F_L) medium (F_M), and high (F_H) FRET states with centers at 0.27, 0.6, and 0.9 from the K125C-S224C labeling sites or at 0.24, 0.52, and 0.78 from the K169C-Q194C labeling sites (Fig. 2*B*). The effects of cholesterol on the S4 conformational dynamics were then analyzed by SPARTAN software (30) using a kinetic model containing four FRET states (Fig. 2*C*). The additional F_B state was added to minimize the impacts of bleaching/blinking events occasionally included. The idealizations of smFRET traces were performed using the maximum point likelihood algorithm (31), which can directly optimize the rate constants of multiple datasets collected at different experimental conditions. In sharp contrast to those without cholesterol, activating voltages of 0 or 120 mV failed to enrich the high FRET 0.9 state at the K125C-S224C sites (Fig. 2*D* and *SI Appendix*, Fig. S3*A*), and their ability to promote the low FRET 0.24 state at the K169C-Q194C labeling sites was also remarkably attenuated in hHv1 channels in liposomes containing 20% cholesterol (Fig. 2*E* and *SI Appendix*, Fig. S3*A*). Our smFRET data consistently suggested that cholesterol inhibits the hHv1 channel by stabilizing the S4 segment at resting conformations.

$Zn^{2\pm}$ and Cholesterol Inhibit the hHv1 Channel Utilizing a Similar Mechanism. Zn^{2+} is an inhibitor of the hHv1 channel that has been extensively studied. We performed smFRET measurements with or without 1 mM Zn^{2+} at different voltages. Our data showed that the FRET at the K125C-S224C labeling sites still exhibited voltage-dependent changes in the presence of 1 mM Zn^{2+}, but the overall distributions were significantly shifted toward the low FRET states, which were not fully reversed, even by the strong activating voltage of 120 mV (Fig. 2*D* and *SI Appendix*, Fig. S3*A*). The smFRET distribution at the K169C-Q194C labeling sites also demonstrated substantial changes by shifting away from the low FRET state that is associated with channel activation (Fig. 2*E* and *SI Appendix*, Fig. S3*A*). Moreover, we confirmed that Zn^{2+} effects were site specific, for no changes were observed on the K125C-K169C labeling sites, which reflect the relative movements between the S1 and S3 segments (*SI Appendix*, Fig. S3*B*). In addition, Zn^{2+} effects at the K125C-S224C labeling sites were significantly impaired by introducing the H140A/H193A mutations, which were reported to reduce Zn^{2+} sensitivity by 200-fold (*SI Appendix*, Fig. S3*C*) (20). Our smFRET data suggested that both cholesterol and Zn^{2+} inhibit the hHv1 channel by modifying the conformational landscapes of the S4 segment.

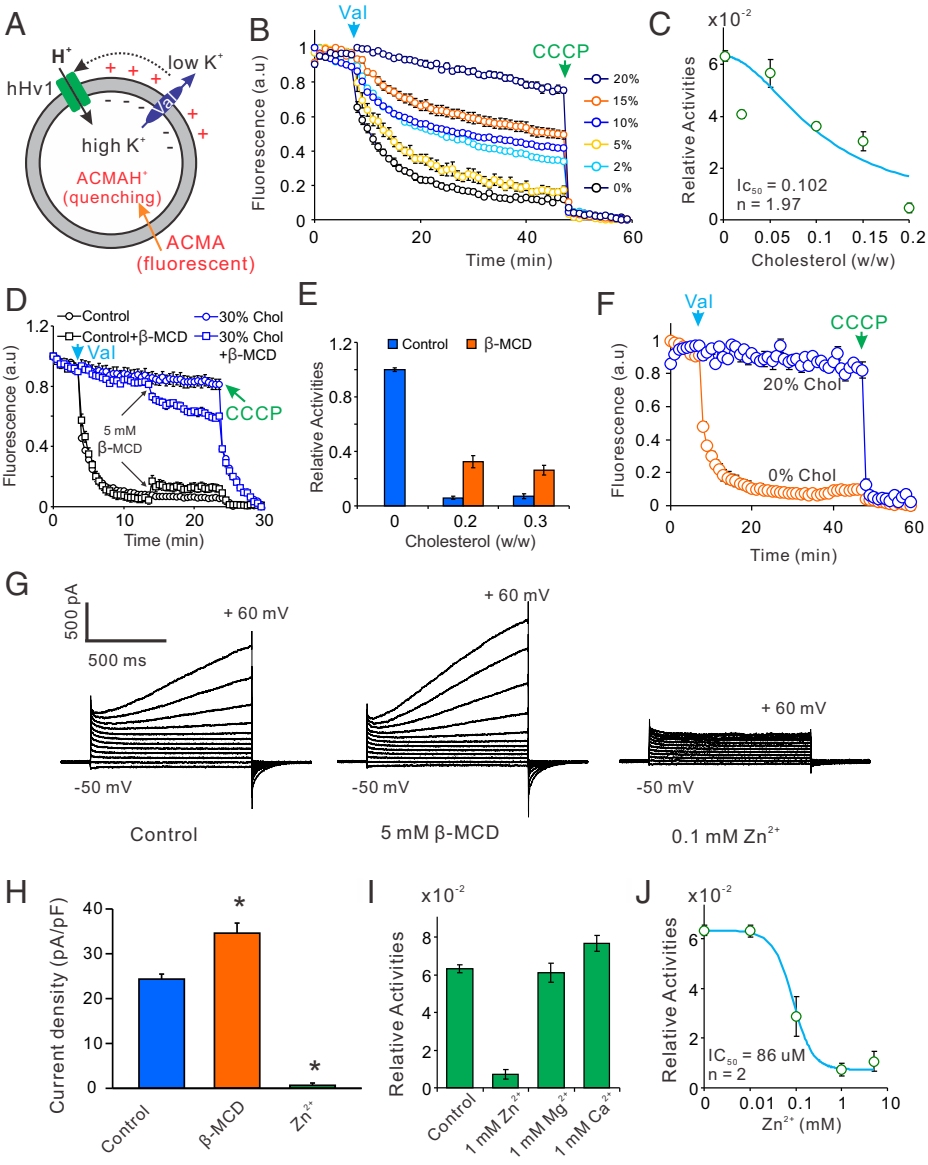

FIG. 1. Cholesterol inhibits the hHv1 channel. (*A*) Liposome flux assay to determine activities of hHv1 channels in liposomes. The electrical potential was generated by the K^+ gradient across liposomes, which drove proton uptake into liposomes, then protonated and quenched the ACMA fluorescence. (*B* and *C*) Dose-dependent inhibition of the hHv1 channel by cholesterol, fitted with the Hill equation. (*D* and *E*) Cholesterol extraction by 5 mM β-MCD attenuated cholesterol inhibition of hHv1 channels. The relative activities of hHv1 channels after adding valinomycin and β-MCD were calculated separately. For the hHv1 liposomes without cholesterol (control), fluorescence quenching reached steady states before adding β-MCD. Therefore, the activities of hHv1 channels in control liposomes after adding β-MCD were not calculated. All data were presented as mean ± SE, $n = 6$. (*F*) Inhibition of the voltage-sensor-only hHv1 channel by 20% cholesterol (wt/wt, to total lipids). Fluorescence intensities were presented as arbitrary unit (a.u). (*G*) The representative whole-cell currents from HEK293 cells transfected with hHv1-EGFP channels. The currents were recorded before and after 5 mM β-MCD treatment, then further validated by exposing to bath solution containing 0.1 mM Zn^{2+} (extracellular side). (*H*) Extraction of membrane cholesterol enhances proton currents through hHv1-EGFP channels expressed in HEK293 cells. All data were presented as mean ± SE, $n = 3$. (*I*) The activities of hHv1 channels in the presence of 1 mM Zn^{2+}, Mg^{2+}, and Ca^{2+}, added to both intra- and extraliposomal sides, were determined by liposome flux assay. (*J*) Dose-dependent inhibition of the hHv1 channel by Zn^{2+}, fitted with the Hill equation. All data were presented as mean ± SE, $n = 3$.

Structural Dynamics Underlying Cholesterol and Zn^{2+} Inhibition of the hHv1 Channel. Kinetic analysis of smFRET data can provide insights into how ligands alter the transition kinetics to shift the conformational landscapes of the S4 segment in the hHv1 channel. We calculated the transition rates of the kinetic model from the idealized smFRET traces at the K125C-S224C and K169C-Q194C labeling sites (Fig. 2 *B* and *C*). Since our smFRET measurements were performed at equilibrium conditions, the ratios of forward to reverse transition rates are the equilibrium constants of the transitions. In our previous work, we showed that only the low-to-high (L2H) transition (i.e., between the low and high FRET states) is highly responsive to membrane voltage and pH changes, which reflects the conformational transitions of the S4 segment between the cytosolic and extracellular sides. In the presence of 20% cholesterol, at the K169C-Q194C labeling sites, even at the strong 120-mV voltage, the equilibrium constant of the L2H transition is still higher than that at −85 mV without cholesterol. Similar changes were also observed at the K125C-S224C labeling sites, but the strong activating voltage of 120 mV appeared to promote the L2H transition equilibrium significantly to a similar level as that of wild type (WT) (Fig. 3). With 1 mM Zn^{2+}, at both K125C-S224C and K169C-Q194C labeling sites, the equilibrium constants of transitions between L2H FRET states are significantly less sensitive to voltages (Fig. 3). Together, these data indicated that cholesterol and Zn^{2+} share a similar structural basis in inhibiting

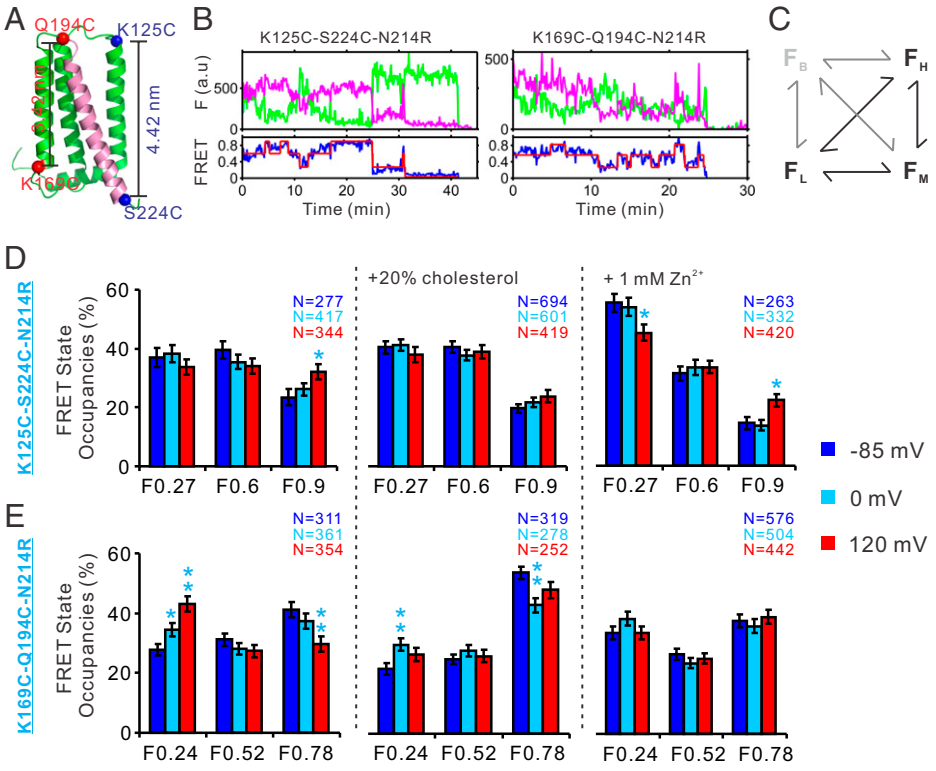

FIG. 2. Cholesterol and Zn^{2+} stabilize the S4 segment at resting conformation. (*A*) Cartoon representation of the hHv1 structure with the S4 segment colored pink, the α-carbons of the K125C-S224C and K169C-Q194C labeling sites were highlighted as blue and red spheres, respectively. For both labeling sites, the N214R background mutation was introduced to abolish proton uptake into liposomes that will alter the voltage dependence of the hHv1 channel (29, 37, 38). (*B*) Representative smFRET traces from the K125C-S224C and K169-Q194C labeling sites. The green and pink lines in the *Upper Panels* are the donor and acceptor intensities, and the blue and red lines in the *Lower Panels* are the measured and idealized FRET. The time resolution of smFRET imaging was 100 ms. (*C*) The kinetic model for analyzing the smFRET traces from the K125-S224C and K169C-Q194C labeling sites. The model was established in our previous work, containing four FRET states, i.e., low (F_L), medium (F_M), high (F_H), and bleaching (F_B) FRET states. The F_B state was introduced to minimize the impact of some FRET events when the donor or acceptor fluorophores were bleached or blinked. (*D* and E) FRET state occupancies calculated from the smFRET data at the K125C-S224C (*D*) and K169C-S194C (*E*) labeling sites. The smFRET traces were idealized based on the four-FRET-state kinetic model using the maximum point likelihood algorithm. The state occupancy data were presented as mean ± SE. Significance levels of FRET state occupancy changes induced by voltage, cholesterol, or Zn^{2+} were examined by unpaired *t* tests, with $^*P < 0.05$ and $^{**}P < 0.01$.

the hHv1 channel by shifting the voltage dependence of the S4 segments.

In summary, our results established the S4 segment as the central gating machinery in hHv1 channels, where all gating factors, including voltage and pH, are converged to modify its conformational landscapes, thus regulating the channel function.

Discussion

In the present work, we established the S4 segment as the central gating machinery that multiple gating factors act on to regulate the hHv1 channel. Our results suggested that cholesterol and Zn^{2+} modify conformational distributions of the S4 segment in hHv1 channels by enriching the inward resting conformations. According to our results, we propose a model that explains the voltage, pH, and ligand gating in the hHv1 channel (Fig. 4*A*). In the model, pH changes the protonation states of intra- and extracellular pH sensing residues that modify the stability of the S4 segment at resting conformation, and the inhibitors, including Zn^{2+} and cholesterol, promote the resting conformation.

We propose that the sperm hHv1 channel may play a central role in regulating human fertilization (Fig. 4*B*). Upon the removal of the Zn^{2+} inhibition in oviducts, cholesterol may provide an important safeguard mechanism to ensure that only the sperm undergoing sufficient cholesterol efflux is hyperactivated to fertilize eggs. The albumin and HDL in female oviductal fluids extract sperm membrane cholesterol to destabilize sperm membranes for fusion with eggs (3). Human albumin, serving dual roles as membrane cholesterol extractor and hHv1 channel activator, collectively opens the hHv1 channel to elevate the intracellular pH (14). As a result, the CatSper channel is activated upon high intracellular pH and progesterone, which triggers calcium influx to hyperactivate sperm (17, 18). After fertilization, the fertilized egg releases Zn^{2+} sparks to inhibit the hHv1 channel in the unfertilized sperm as a safeguard mechanism to prevent polyspermy (32). It is worth noting that the intracellular pH of sperm cells is also regulated by other mechanisms, such as Na^+/H^+ exchanger and HCO_3^- transporters (2). In mouse sperm, the Hv1 channel is not even expressed (12). Therefore, cholesterol regulation of the hHv1 channel perhaps is not a universal mechanism for sperm cells of different species, and cholesterol efflux may also regulate sperm cell pH through Na^+/H^+ exchanger and HCO_3^- transporters (33–35). Our findings propose that HDL and albumin levels could be important maternity factors that may be associated with difficulty conceiving or infertility. The hHv1 channels are expressed in many other cells, like phagocytes, cancer, and glial cells, where cholesterol levels were found to impact their immune responses, cancer invasiveness, or brain ischemic damages (16). Our results imply that the cholesterol effects may partially be due to their inhibitory effects on the hHv1 channel.

Methods

Protein Expression, Purification, and Fluorophore Labeling. Expression and purification of the hHv1 proteins were performed as described previously (29, 36). For smFRET imaging, the two intrinsic cysteine residues C107 and

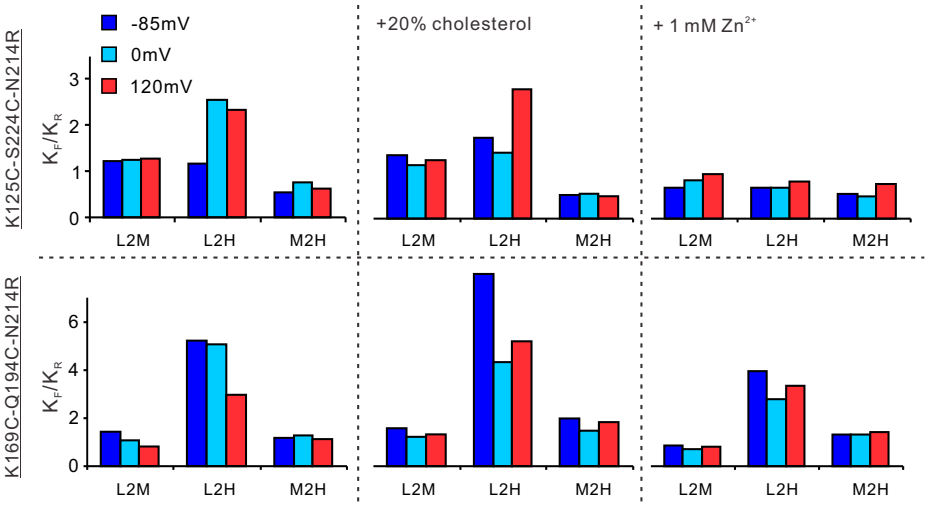

FIG. 3. Effects of voltage, cholesterol, and Zn^{2+} on the conformational dynamics of the S4 segment revealed by equilibrium constants. The transitions among the F_L, F_M, and F_H states were classified into F_L to F_M (L2M), F_L to F_H (L2H), and F_M to F_H (M2H) transitions. The equilibrium constants of the three different transition types were calculated as the ratios of its forward to reverse transition rates for our smFRET data were collected from the K125C-S224C and K169C-Q194C labeling sites at equilibrium voltage/ligand conditions. Among the three different transitions, only the equilibrium constants between the F_L and F_H states, i.e., L2H, are highly responsive to voltage, Zn^{2+}, and cholesterol, which reflect the transitions of the S4 segment between the inward resting and outward activating conformations.

C249 of the hHv1 channel were mutated into Ser and then double cysteine mutations were introduced at the K125/S224 or K169/Q194 sites, with the additional N214R background mutation that abolishes proton uptake into liposomes (29, 37, 38). The modified Cy3 and Cy5 c5 maleimide fluorophores with improved photostability were used to label the cysteine residue pair introduced into the hHv1 channel, one pair at a time, as described previously (29, 39). The EGFP-hHv1 fusion channel was constructed by fusing the EGFP tag to the N terminus of the hHv1 channel with a flexible "GGSGS" linker. All purified hHv1 proteins were either reconstituted into liposomes immediately or flash frozen in liquid nitrogen and then stored at −80 °C for later use.

hHv1 Liposome Reconstitution. The hHv1 mutant proteins, including those carrying the cysteine mutations at different sites, were reconstituted into liposomes (POPE/POPG, 3:1) containing 20% (wt/wt, to total lipids) cholesterol at a protein-to-total-lipids ratio of 1:200 (wt/wt) for liposome flux assays. For smFRET imaging, the protein-to-total-lipids ratio was reduced to 1:4,000 (wt/wt) so that most liposomes were either empty or contained only one hHv1 channel protein (29). Divalent cations, including Zn^{2+}, were loaded to both extra- and intraliposomal sides with brief sonication after reconstitution. The hHv1 proteoliposomes were either used immediately or flash frozen with liquid nitrogen and stored in a −80 °C freezer for later use.

Liposome Fluorescence Flux Assay. The K^+ gradient across liposomes was established by 10× dilution of liposomes with K^+ free buffer containing 20 mM 4-(2-hydroxyethyl)-1-piperazineethanesulfonic acid (HEPES), 150 mM *N*-methyl-D-glucamine, pH 7.5. The liposomes were incubated with 2 μM of ACMA fluorescence probes for ∼5 min, then ACMA fluorescence was measured using a 96-well plate reader (FluoStar, Ex/Em = 390 nm/460 nm) for ∼5 min.

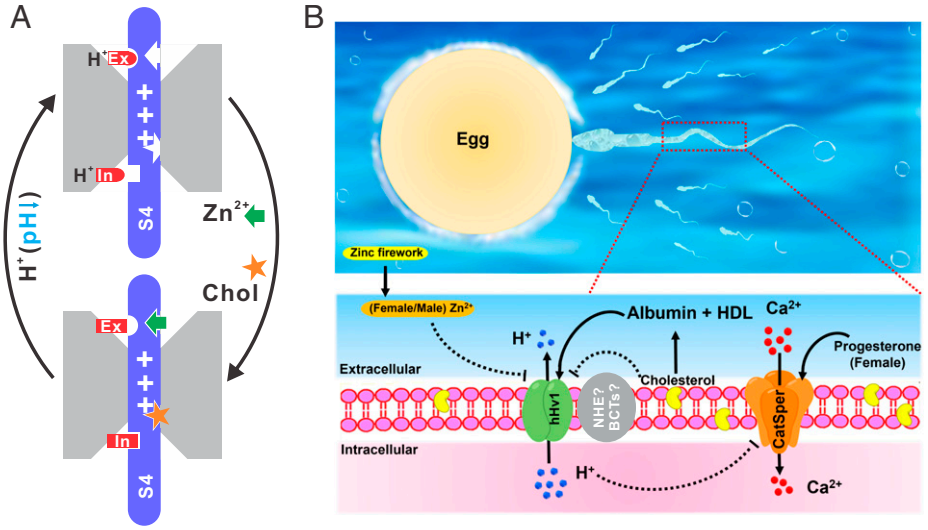

FIG. 4. The structural basis underlying ligand regulation of hHv1 channels and its potential roles in fertilization. (*A*) The structural basis underlying ligand regulation of hHv1 channels. The protonation states of the pH-sensing residues at the intra- (In) or extracellular (Ex) sides change their interactions with the resting state S4 segment to which Zn^{2+} (green arrow) and cholesterol (orange star) also bind. (*B*) The potential role of the hHv1 channel in human fertilization. The cholesterol efflux is facilitated by HDL and albumin in the oviductal fluid. Removal of membrane cholesterol and the presence of albumin collectively activate the sperm hHv1 channel, leading to efflux of protons and thus elevation of intracellular pH. Progesterone and high intracellular pH activate the CatSper channel to facilitate calcium influx, which leads to hyperactivation of sperm for fertilization. The fertilized egg generates Zn^{2+} fireworks, which inhibit hHv1 channels of the surrounding unfertilized sperm to prevent polyspermy. However, cholesterol efflux may impact sperm cell pH through other pathways, like Na^+/H^+ exchanger (NHE) and HCO_3^- transporters (bicarbonate transporters [BCTs]) in other species, especially for mouse sperm that does not express Hv1 channels.

After valinomycin was added at a final concentration of 0.45 μM, the fluorescence measurements were resumed with the same optical setting for ∼30 min. The fluorescence liposome flux data were processed following the method of Su et al. (40). In brief, the hHv1 channel activities were calculated from the fluorescence readings normalized between 0 and 1 using the equation

$$A = (F_0 - F_{val})/(F_0 - F_{cccp}),$$

where F_0, F_{val}, and F_{cccp} were the steady-state ACMA fluorescence at initial, after adding valinomycin and CCCP, respectively. The relative activities of hHv1 channels were calculated as rates of ACMA fluorescence quenching. The hHv1 WT proteoliposomes were included in every batch of assays for normalization.

smFRET Imaging and Kinetic Analysis. Flow chambers for smFRET imaging were prepared following the protocol of Joo et al., with coverslip surfaces coated with polyethylene glycol (PEG) containing 2% biotin-PEG (41). The biotinylated anti-Histag antibodies (ThermoFisher, MA1-21315-BTIN) were attached to biotin-PEG coverslip surfaces through neutravidin (29). Since most liposomes were either empty or containing only 1 hHv1 channel, only the hHv1 liposomes with the cytoplasmic Histag facing the extraliposomal side were retained by anti-Histag antibodies for smFRET imaging. smFRET imaging was performed with an objective-based total internal reflection fluorescence (TIRF) microscope, and liposome voltages were generated by transliposomal K^+ gradients in the presence of 0.45 μM valinomycin as described previously (29, 42). A 532 nm laser (∼1.0 W/cm^2) was used to collect smFRET movies at 10 frames per second, and a 640 nm laser (∼1.0 W/cm^2) was only used to confirm the existence of acceptor fluorophore. For each sample/condition, at least three independent batches of smFRET movies were collected. All imaging buffers contained ∼3 mM Trolox, 5 mM PCA, and 15 μg/μL of protocatechuate 3,4-dioxygenase to enhance the photostability of the fluorophores (43, 44). The smFRET traces were identified and extracted from the raw smFRET movies without any corrections using the SPARTAN software, with the point spread function window size of seven pixels (30). All smFRET traces were automatically selected by the Autotrace function of SPARTAN software, using settings including FRET Lifetime >50 frames, donor/acceptor correlation coefficient between −1.1 and 0.5, signal-to-noise ratio >8, background ground noise <70, donor blinks <4, and overlap molecule-removal function checked. The selected traces were further manually inspected to ensure that donor and acceptor fluorophores did not show more than one bleaching step and exhibited a clear anticorrelation pattern (29, 45, 46). The smFRET traces were heterogenic, with over 40% of smFRET traces exhibiting transitions among more than three FRET states. All smFRET traces from the same labeling site and experimental condition were included in kinetic analyses, following the procedure described in our previous work with SPARTAN software (30). A four-FRET-state model (Fig. 2*C*) was used for all kinetic analyses, and the maximum point likelihood algorithm was used for optimizing transition rate constants (31).

Patch-Clamp Electrophysiology. The hHv1-EGFP cDNA encoding a hHv1 channel carrying a carboxyl-terminal EGFP fusion tag, connected by a double "GGS" flexible linker, was subcloned into the pAS vector (Addgene No. 140008) for expression in HEK293 cells. HEK293 cells were cultured in the DMEM supplied with 10% fetal bovine serum and 100 U penicillin/streptomycin. The hHv1-EGFP plasmids were transfected into HEK293 cells using Lipofectamine 3000 reagent (Invitrogen Inc.). Patch-clamp recordings were performed under whole-cell mode on the transfected cells 1∼2 d after, as described by Musset et al. (11). In brief, the pipette solution contained 100 mM tetramethylammonium bromide, 100 mM cesium methanesulfonate, 1 mM ethylene glycol-bis(β-aminoethyl ether)-N,N,N′,N′-tetraacetic acid, and 2 mM $MgCl_2$. The pH of the pipette solution was adjusted to 6.2 by 2-(N-morpholino)ethanesulfonic acid, and the osmolarity was adjusted to 295 mOsm/L by methanesulfonic acid. The bath solution was used as described previously (47), containing 140 mM NaCl, 5.4 mM KCl, 10 mM glucose, 20 mM HEPES, 2.0 mM $CaCl_2$, and 1.0 mM $MgCl_2$. The pH was adjusted to 7.4 by NaOH, and the osmolarity was adjusted to 305 mOsm/L by sucrose. The voltage steps of 10 mV, from −50 to 60 mV, were applied. For cholesterol depletion, 5 mM β-MCD was added to the bath solution, and 0.1 mM $ZnCl_2$ was used after cholesterol extraction to confirm the specificity of the hHv1 proton currents. No visible current was recorded from cells lacking GFP fluorescence.

Data, Materials, and Software Availability. All data are included in the manuscript and/or supporting information.

ACKNOWLEDGMENTS. This work was funded by NIH grant 1R15GM137215-01 (S.W.) and the startup fund of University of Missouri-Kansas City. The work was also supported, in part, by a grant from American Heart Association (19AIREA34470007) to X.-P.C.

1. N. L. Cross, Role of cholesterol in sperm capacitation. *Biol. Reprod.* **59**, 7–11 (1998).
2. L. C. Puga Molina *et al.*, Molecular basis of human sperm capacitation. *Front. Cell Dev. Biol.* **6**, 72 (2018).
3. T. Leahy, B. M. Gadella, New insights into the regulation of cholesterol efflux from the sperm membrane. *Asian J. Androl.* **17**, 561–567 (2015).
4. B. K. Davis, Interaction of lipids with the plasma membrane of sperm cells. I. The antifertilization action of cholesterol. *Arch. Androl.* **5**, 249–254 (1980).
5. B. K. Davis, R. Byrne, K. Bedigian, Studies on the mechanism of capacitation: Albumin-mediated changes in plasma membrane lipids during in vitro incubation of rat sperm cells. *Proc. Natl. Acad. Sci. U.S.A.* **77**, 1546–1550 (1980).
6. A. J. Travis, G. S. Kopf, The role of cholesterol efflux in regulating the fertilization potential of mammalian spermatozoa. *J. Clin. Invest.* **110**, 731–736 (2002).
7. N. L. Cross, P. Razy-Faulkner, Control of human sperm intracellular pH by cholesterol and its relationship to the response of the acrosome to progesterone. *Biol. Reprod.* **56**, 1169–1174 (1997).
8. M. Sasaki, M. Takagi, Y. Okamura, A voltage sensor-domain protein is a voltage-gated proton channel. *Science* **312**, 589–592 (2006).
9. I. S. Ramsey, M. M. Moran, J. A. Chong, D. E. Clapham, A voltage-gated proton-selective channel lacking the pore domain. *Nature* **440**, 1213–1216 (2006).
10. V. V. Cherny, V. S. Markin, T. E. DeCoursey, The voltage-activated hydrogen ion conductance in rat alveolar epithelial cells is determined by the pH gradient. *J. Gen. Physiol.* **105**, 861–896 (1995).
11. B. Musset *et al.*, Detailed comparison of expressed and native voltage-gated proton channel currents. *J. Physiol.* **586**, 2477–2486 (2008).
12. P. V. Lishko, Y. Kirichok, The role of Hv1 and CatSper channels in sperm activation. *J. Physiol.* **588**, 4667–4672 (2010).
13. A. Kawanabe, Y. Okamura, Effects of unsaturated fatty acids on the kinetics of voltage-gated proton channels heterologously expressed in cultured cells. *J. Physiol.* **594**, 595–610 (2016).
14. R. Zhao *et al.*, Direct activation of the proton channel by albumin leads to human sperm capacitation and sustained release of inflammatory mediators by neutrophils. *Nat. Commun.* **12**, 3855 (2021).
15. V. V. Cherny, T. E. DeCoursey, pH-dependent inhibition of voltage-gated H(+) currents in rat alveolar epithelial cells by Zn(2+) and other divalent cations. *J. Gen. Physiol.* **114**, 819–838 (1999).
16. T. E. DeCoursey, Voltage-gated proton channels: Molecular biology, physiology, and pathophysiology of the H(V) family. *Physiol. Rev.* **93**, 599–652 (2013).
17. P. V. Lishko, I. L. Botchkina, A. Fedorenko, Y. Kirichok, Acid extrusion from human spermatozoa is mediated by flagellar voltage-gated proton channel. *Cell* **140**, 327–337 (2010).
18. P. V. Lishko, I. L. Botchkina, Y. Kirichok, Progesterone activates the principal Ca^{2+} channel of human sperm. *Nature* **471**, 387–391 (2011).
19. T. Strünker *et al.*, The CatSper channel mediates progesterone-induced Ca^{2+} influx in human sperm. *Nature* **471**, 382–386 (2011).
20. B. Musset *et al.*, Zinc inhibition of monomeric and dimeric proton channels suggests cooperative gating. *J. Physiol.* **588**, 1435–1449 (2010).
21. F. Qiu *et al.*, Molecular mechanism of Zn^{2+} inhibition of a voltage-gated proton channel. *Proc. Natl. Acad. Sci. U.S.A.* **113**, E5962–E5971 (2016).
22. V. V. Cherny *et al.*, Engineered high-affinity zinc binding site reveals gating configurations of a human proton channel. *J. Gen. Physiol.* **152**, e202012664 (2020).
23. G. Chaves, S. Bungert-Plümke, A. Franzen, I. Mahorivska, B. Musset, Zinc modulation of proton currents in a new voltage-gated proton channel suggests a mechanism of inhibition. *FEBS J.* **287**, 4996–5018 (2020).
24. B. H. Falkenburger, J. B. Jensen, E. J. Dickson, B. C. Suh, B. Hille, Phosphoinositides: Lipid regulators of membrane proteins. *J. Physiol.* **588**, 3179–3185 (2010).
25. I. Levitan, D. K. Singh, A. Rosenhouse-Dantsker, Cholesterol binding to ion channels. *Front. Physiol.* **5**, 65 (2014).
26. S. Y. Lee, J. A. Letts, R. MacKinnon, Functional reconstitution of purified human Hv1 H+ channels. *J. Mol. Biol.* **387**, 1055–1060 (2009).
27. S. Sankaranarayanan *et al.*, Serum albumin acts as a shuttle to enhance cholesterol efflux from cells. *J. Lipid Res.* **54**, 671–676 (2013).
28. L. Hong, I. H. Kim, F. Tombola, Molecular determinants of Hv1 proton channel inhibition by guanidine derivatives. *Proc. Natl. Acad. Sci. U.S.A.* **111**, 9971–9976 (2014).
29. S. Han *et al.*, Structural dynamics determine voltage and pH gating in human voltage-gated proton channel. *eLife* **11**, e73093 (2022).
30. M. F. Juette *et al.*, Single-molecule imaging of non-equilibrium molecular ensembles on the millisecond timescale. *Nat. Methods* **13**, 341–344 (2016).
31. F. Qin, A. Auerbach, F. Sachs, A direct optimization approach to hidden Markov modeling for single channel kinetics. *Biophys. J.* **79**, 1915–1927 (2000).
32. E. L. Que *et al.*, Quantitative mapping of zinc fluxes in the mammalian egg reveals the origin of fertilization-induced zinc sparks. *Nat. Chem.* **7**, 130–139 (2015).
33. C. E. Poli de Figueiredo *et al.*, Modulation of Na-H antiporter activity in human lymphoblasts by altered membrane cholesterol. *Am. J. Physiol.* **261**, C1138–C1142 (1991).
34. L. C. Puga Molina *et al.*, Essential role of CFTR in PKA-dependent phosphorylation, alkalinization, and hyperpolarization during human sperm capacitation. *J. Cell. Physiol.* **232**, 1404–1414 (2017).
35. A. Touré, Importance of SLC26 transmembrane anion exchangers in sperm post-testicular maturation and fertilization potential. *Front. Cell Dev. Biol.* **7**, 230 (2019).

36. Q. Li *et al.*, Resting state of the human proton channel dimer in a lipid bilayer. *Proc. Natl. Acad. Sci. U.S.A.* **112**, E5926–E5935 (2015).
37. V. De La Rosa, I. S. Ramsey, Gating currents in the Hv1 proton channel. *Biophys. J.* **114**, 2844–2854 (2018).
38. E. M. Carmona *et al.*, Gating charge displacement in a monomeric voltage-gated proton (H_v1) channel. *Proc. Natl. Acad. Sci. U.S.A.* **115**, 9240–9245 (2018).
39. Q. Zheng *et al.*, Electronic tuning of self-healing fluorophores for live-cell and single-molecule imaging. *Chem. Sci. (Camb.)* **8**, 755–762 (2017).
40. Z. Su, E. C. Brown, W. Wang, R. MacKinnon, Novel cell-free high-throughput screening method for pharmacological tools targeting K^+ channels. *Proc. Natl. Acad. Sci. U.S.A.* **113**, 5748–5753 (2016).
41. C. Joo, T. Ha, Preparing sample chambers for single-molecule FRET. *Cold Spring Harb. Protoc.* **2012**, 1104–1108 (2012).
42. S. Wang *et al.*, Potassium channel selectivity filter dynamics revealed by single-molecule FRET. *Nat. Chem. Biol.* **15**, 377–383 (2019).
43. C. E. Aitken, R. A. Marshall, J. D. Puglisi, An oxygen scavenging system for improvement of dye stability in single-molecule fluorescence experiments. *Biophys. J.* **94**, 1826–1835 (2008).
44. R. Dave, D. S. Terry, J. B. Munro, S. C. Blanchard, Mitigating unwanted photophysical processes for improved single-molecule fluorescence imaging. *Biophys. J.* **96**, 2371–2381 (2009).
45. S. Wang, R. Vafabakhsh, W. F. Borschel, T. Ha, C. G. Nichols, Structural dynamics of potassium-channel gating revealed by single-molecule FRET. *Nat. Struct. Mol. Biol.* **23**, 31–36 (2016).
46. S. Wang, J. B. Brettmann, C. G. Nichols, "Studying structural dynamics of potassium channels by single-molecule FRET" in *Potassium Channels*, S. L. Shyng, F. I. Valiyaveetil, M. Whorton, Eds. (Springer, 2018), pp. 163–180.
47. Q. Jiang *et al.*, Histidine residues are responsible for bidirectional effects of zinc on acid-sensing ion channel 1a/3 heteromeric channels. *Biomolecules* **10**, 1264 (2020).